ChemPubSoc Europe

DOI: 10.1002/chem.201406582

CHEMISTRY
A European Journal
Full Paper

Heterojunction Nanocrystals

Facile Synthesis of Quasi-One-Dimensional Au/PtAu Heterojunction Nanotubes and Their Application as Catalysts in an Oxygen-Reduction Reaction

Kai Cai, Jiawei Liu, Huan Zhang, Zhao Huang, Zhicheng Lu, Mohamed F. Foda, Tingting Li, and Heyou Han*[a]

Abstract: An intermediate-template-directed method has been developed for the synthesis of quasi-one-dimensional Au/PtAu heterojunction nanotubes by the heterogeneous nucleation and growth of Au on Te/Pt core–shell nanostructures in aqueous solution. The synthesized porous Au/PtAu bimetallic nanotubes (PABNTs) consist of porous tubular framework and attached Au nanoparticles (AuNPs). The reaction intermediates played an important role in the preparation, which fabricated the framework and provided a localized reducing agent for the reduction of the Au and Pt precursors. The Pt_7Au PABNTs showed higher electrocatalytic activity and durability in the oxygen-reduction reaction (ORR) in 0.1 M $HClO_4$ than porous Pt nanotubes (PtNTs) and commercially available Pt/C. The mass activity of PABNTs was 218% that of commercial Pt/C after an accelerated durability test. This study demonstrates the potential of PABNTs as highly efficient electrocatalysts. In addition, this method provides a facile strategy for the synthesis of desirable heteronanostructures with controlled size and shape by utilizing an intermediate template.

Introduction

Heterojunction nanocrystals (HNCs) have received great interest as they exhibit novel or improved physical and chemical properties and are expected to play a crucial role in many fields, such as nanoscale electronic and electrochemical devices.[1–3] So far, many HNCs, including dumbbell-like, core-shell, and branched nanostructures, have been reported.[4–7] Pt-based materials are the leading electrocatalysts for the reduction of oxygen in proton-exchange membrane fuel cells (PEMFCs).[8–9] Because of the high cost and limited total storage of Pt, the development of a more efficient Pt-based electrocatalyst has become increasingly important.[10–15] The use of another metal species to fabricate heterostructures is an alternative method.[10,11,16] Over recent decades, Pt-based HNCs have been extensively studied as highly efficient electrocatalysts.[10,11,16–23] For example, Pt–Pd and Pt–Au HNCs have been synthesized by different research groups and demonstrated to improve the electrocatalytic activities for the oxygen-reduction or fuel-oxidation reaction.[17–23]

One-dimensional (1D) nanocrystals, such as nanowires and nanotubes, have better electrical transport and are less vulnerable to dissolution and aggregation than zero-dimensional (0D) nanocrystals when used as self-supported electrocatalysts.[24–27] However, there has been little research into 1D Pt-based HNCs and their catalytic activities, especially heterostructured nanotubes.[27–29] As we know, Pt nanotubes are generally obtained by using templates, including inorganic nanowires and organic and viral templates because of their extremely high surface energy.[24–26,30,31] Very recently, our group synthesized porous Pt nanotubes by using Te nanowires as templates at room temperature.[31] In the synthesis, a protective atmosphere and heating are not required. More importantly, porous hollow nanostructures were finally obtained. Although there have been many Pt-based nanostructures synthesized with Te nanowires as a template,[27,28,31–38] there is no report of the successful preparation of HNCs containing porous nanotubes and nanoparticles until now. In addition, Au catalysts are more stable than Pd catalysts; furthermore, it has been demonstrated that Au species can promote the performance of Pt catalysts for electrocatalytic reactions.[20–23] Therefore, it is desirable and meaningful to develop a new strategy for the synthesis of Pt-based HNCs including Au.

Herein, we presented a facile synthesis of quasi-1D Pt-based HNCs containing Au nanoparticles. By the heteroepitaxial growth of Au on Te/Pt core–shell nanostructures under controlled conditions, porous Au/PtAu bimetallic nanotubes (PABNTs) were obtained. The skeleton of the novel HNCs comprises PtAu bimetallic porous nanotubes on which Au nanoparticles are attached. The Te/Pt core–shell nanostructures play a crucial role in the process because these structures serve as a framework and provide a localized reducing agent for the re-

[a] K. Cai,[+] J. Liu,[+] H. Zhang, Z. Huang, Dr. Z. Lu, M. F. Foda, T. Li, Prof. H. Han
State Key Laboratory of Agriculture Microbiology
College of Science, College of Food Science and Technology
Huazhong Agricultural University, Wuhan 430070 (P.R. China)
E-mail: hyhan@hzau.edu.cn

[+] These authors contributed equally to this work.

Supporting information for this article is available on the WWW under http://dx.doi.org/10.1002/chem.201406582.

duction of the Au precursor, for which no other reductants are required. We further studied the electrocatalysis of the HNCs toward the oxygen-reduction reaction (ORR). As expected, the HNCs showed a much higher catalytic activity and durability than porous PtNTs and commercial Pt/C. This study should provide new insight into a strategy that uses templates to obtain HNCs with enhanced properties.

Results and Discussion

Preparation and characterization of PABNTs

A typical preparation of PABNTs was performed by using the following procedure: First, Te nanowires (NWs) were prepared according to a previous method.[39] The Te/Pt core–shell nanostructures were fabricated by using TeNWs as partially sacrificial templates in aqueous solution. After that, a certain amount of $HAuCl_4$ was added into the previous solution to obtain PABNTs. During the process, AuNPs heterogeneously nucleated and grew epitaxially on the shell of the intermediate along with the formation of a great number of Au atoms because of the rapid redox reaction between the elemental Te and $HAuCl_4$. Meanwhile, PtAu bimetallic nanotubes were formed because a partial Au was widely deposited on the shell.

TeNWs were synthesized with a mean diameter of 18 nm and a length of 350 nm (Figure 1 A). Figure 1 B shows a typical TEM image of the PABNTs, with skeletons of the same dimensions as the TeNWs templates and all decorated by NPs. In addition, there are no individual NPs in the surroundings, thus suggesting that the NPs heterogeneously nucleate and grow directly on the surface of the framework. The enlarged magnification in Figure 1 C and high-resolution (HR) TEM in Figure 1 D shows that the nanotubes are composed of interconnected tiny NPs and the adjacent lattice fringe of the attached particle is approximately 0.24 nm, which corresponds to the lattice spacing of the (111) lattice planes in face-centered-cubic Au structures.

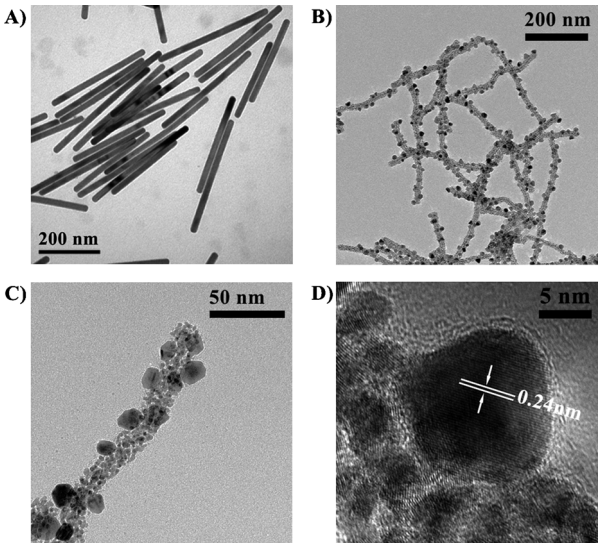

Figure 1. TEM images of A) TeNWs and B,C) PABNTs. D) HRTEM image of PABNTs (Pt_2Au).

The nanostructures were further characterized by high-angle annular dark-field (HAADF) scanning transmission electron microscopy (STEM). Figure 2 A shows the HAADF-STEM images of the nanostructures. Panels a and b in Figure 2 B give the elemental mappings of panel c, which is the outlined section in Figure 2 A. Obviously, elemental Au was distributed on every

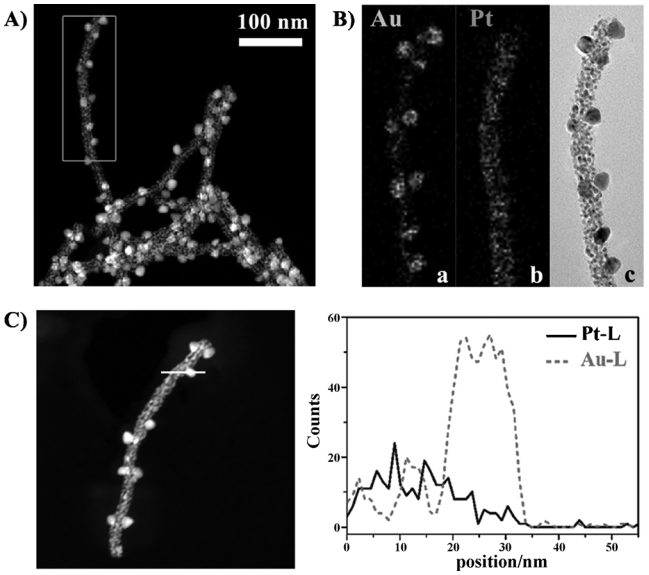

Figure 2. A) HAADF-STEM images and B) HAADF-STEM energy-dispersive X-ray spectroscopy (EDX) mapping image of PABNTs (Pt_2Au). C) Cross-sectional compositional line profiles of the corresponding lines for Pt and Au in the nanotubes. Pt_2Au denotes that the atom ratio of Pt/Au = 2:1. The quality of the PABNTs was analyzed by ICP-AES.

component containing the skeleton and all the NPs, whereas elemental Pt was distributed mainly on the skeleton. Moreover, the cross-sectional line profiles of the corresponding compositions on individual PABNTs reveal an identical result (Figure 2 C). XRD patterns show that both the Pt and Au crystals are face-centered-cubic (fcc) structures (Figure 3). The fact that the peaks of the (fcc) Au crystals are higher accounts for the larger crystalline grain of Au in the structures, which is in accordance with the TEM analysis. In addition, the UV/Vis absorption spectra of PABNTs show an absorption band at around $\lambda =$ 520 nm attributed to the AuNPs (Figure 4).

The quality of the PABNTs was analyzed by inductively coupled plasma atomic emission spectroscopy (ICP-AES). The molar ratio of Pt/Au in PABNTs is about 2:1, which is different from the precursor ratio because the $AuCl_4^-$ ion has a higher galvanic replacement reaction rate than the $[PtCl_6]^{2-}$ ion. When the precursor ratio of Pt/Au was regulated, the molar ratio of Pt/Au in the new PABNTs was about 7:1 according to ICP-AES analysis. TEM images indicated that the NPs have an obviously decreased size (see Figure S1 in the Supporting Information). The XRD pattern shows lower peaks for the Au crystals and the absorption band of the Au species becomes indistinct in the UV/Vis absorption spectra (Figures 3 and 4, respectively).

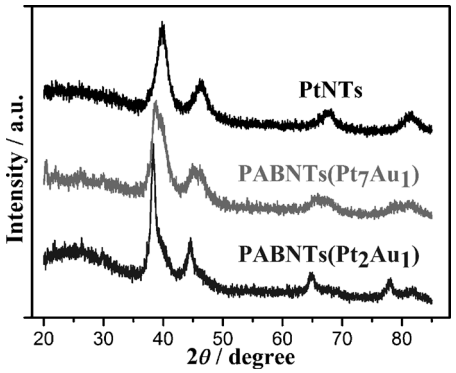

Figure 3. XRD patterns of PtNTs, PABNTs (Pt_2Au), and PABNTs (Pt_7Au). Pt_2Au and Pt_7Au denote that the atom ratios of Pt/Au = 2:1 and 7:1, respectively.

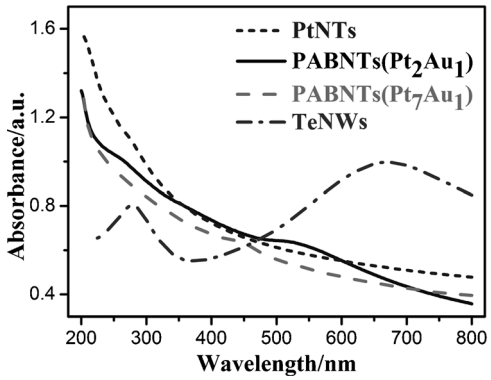

Figure 4. UV/Vis absorption spectra of the TeNWs, PtNTs, and PABNTs.

The HAADF-STEM images and the cross-sectional line profiles of the individual NTs show that the NPs consist of Au, whereas the NTs consist of Pt and Au (see Figure S2 in the Supporting Information).

It is noteworthy that the reaction intermediates, namely, the Te/Pt core–shell nanostructures, played an important role in the preparation of the PABNTs. These nanostructures fabricated the framework and provided a localized reducing agent for the reduction of the Au and Pt precursors. When the Au and Pt precursors were added simultaneously, only bimetallic nanoparticles were obtained, which is in accordance with a previous study (see Figure S3 in the Supporting Information).[32] However, heterostructures could be obtained if the intermediates were fabricated before the addition of the Au precursor. The shells of the intermediates were initially formed and the core partly disintegrated because of its instability (see Figure S4 A in the Supporting Information). Moreover, there is no need to add another reducing agent to the solvent in the synthesis. If no Au precursor was added, porous PtNTs would be obtained because the core spontaneously disintegrated and diffused (see Figure S4 B in the Supporting Information).

Electrocatalytic activity of PABNTs

The PABNTs with an atom ratio of Pt/Au of 7:1 (Pt_7Au) were used as a catalyst to measure the electrocatalytic activity. Meanwhile, porous PtNTs and commercial Pt/C were used for comparison. Figure 5 A shows the cyclic voltammetry (CV) curves of PABNTs, PtNTs, and Pt/C recorded in N_2-purged 0.1 M $HClO_4$ solutions at 25 °C versus the Ag/AgCl electrode, with a scan rate of 50 mV s^{-1}. The hydrogen adsorption/desorption region appeared in the range −0.2–0.15 V, which was used to estimate the electrochemically active surface area (ECSA) of the electrocatalyst by measuring the charge collected in this region after double-layer correction and assuming a value of 210 μC cm^{-2} for the adsorption of a hydrogen monolayer. The metal oxidation/reduction region was 0.4–0.8 V. The specific ECSA values (i.e., the ECSA per unit weight of Pt) were 22.3, 23.6, and 59.9 m^2g^{-1} for PABNTs, PtNTs, and Pt/C, respectively. The lower ECSA values of the PABNTs and PtNTs are probably due to their intrinsic 1D morphology, which is in accordance with the results of previous studies.[24,26,40]

The ORR tests of PABNTs, PtNTs, and Pt/C were conducted in an O_2-saturated solution of 0.1 M $HClO_4$ at a sweep rate of 10 mV s^{-1}. The ORR polarization curves show that the region of

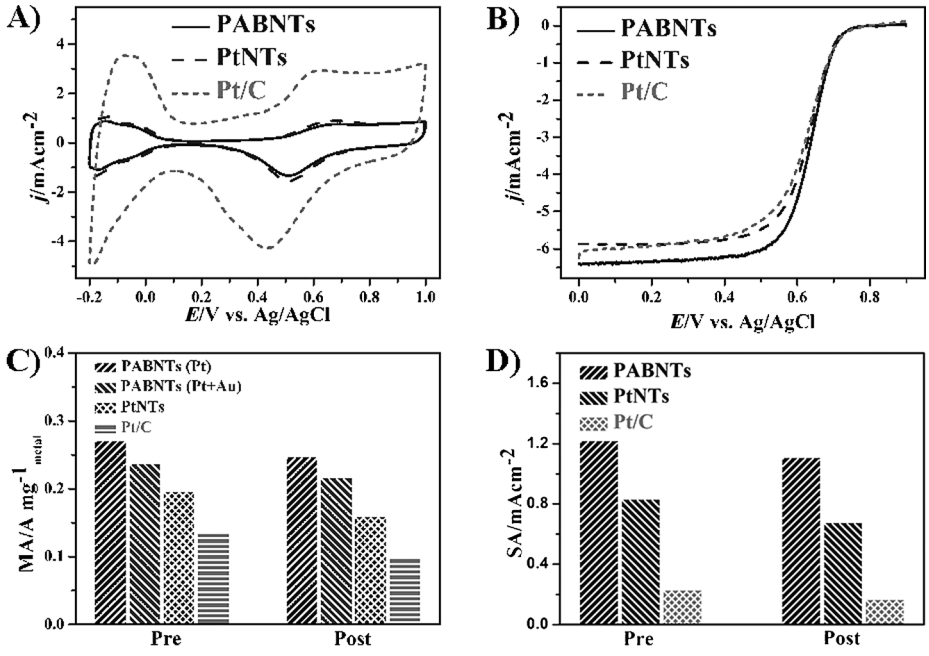

Figure 5. A) CV of N_2-purged aqueous solutions of 0.1 M $HClO_4$ versus the Ag/AgCl electrode, B) polarization curves of O_2-saturated aqueous solutions of 0.1 M $HClO_4$, C) summary of the ORR mass activities, and D) specific activities of PABNTs, PtNTs, and commercial Pt/C at 600 mV before and after an accelerated durability test.

the diffusion-limiting current is between 0 and 0.55 V and the mixed kinetic-diffusion-controlled region ranges from 0.55 to 0.75 V. The mass activities (MA) and specific activities (SA) are given as kinetic current densities (j_k), which were calculated according to the Koutecky–Levich equation and normalized in reference to the loading amount and ECSA of the metal, respectively. Polarization curves show that PABNTs have a more positive onset potential (Figure 5B). PABNTs have a higher MA than PtNTs and commercial Pt/C (0.237 A $mg_{(Pt+Au)}^{-1}$, 0.196 A $mg_{(Pt)}^{-1}$, and 0.136 A $mg_{(Pt)}^{-1}$; Figure 5C). The intrinsic activities of the electrocatalysts were represented by the area-specific kinetic current densities (Figure 5D). PABNTs have a SA of 1.218 mA cm^{-2} at 600 mV, which is more than fivefold that of Pt/C (0.227 mA cm^{-2}) and are nearly 1.5-fold that of the PtNTs (0.830 mA cm^{-2}). Due to the high specific area of the porous nanostructures, the surface of the catalysts is probably more easily accessible for O_2 absorption and activation. In addition, the interface-lattice mismatch between the Pt and Au species can lead to surface strain in the PABNTs, which may play an important role in enhancing the ORR activity.[11]

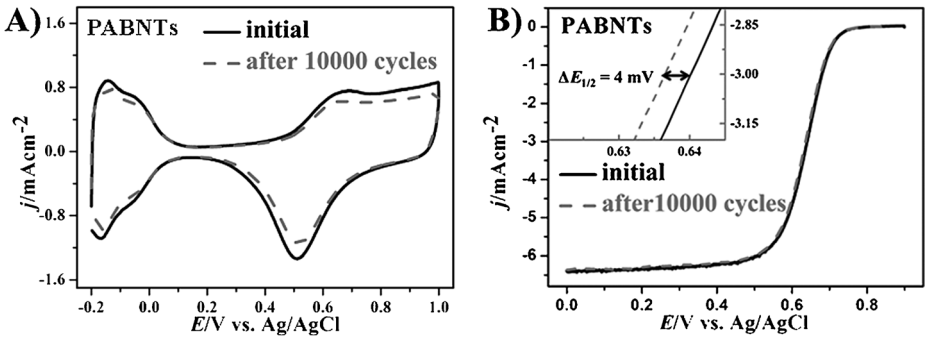

Figure 6. A) CV and B) polarization curves for PABNTs before and after an accelerated durability test in fresh aqueous solution of $HClO_4$.

Figure 6A shows the 1st and 10000th CV curves of the PABNTs. The CV measurements showed that after 10000 cycles there was a loss of 8.9% in ECSA for the PABNTs, whereas the decrease of the ECSA in PtNTs and Pt/C is 11.0 and 17.3%, respectively (see Figures S5A and S6A in the Supporting Information, respectively). The ORR activities of these catalysts before and after the durability test are shown in Figure 6B and Figures S5B and S6B in the Supporting Information. The PABNTs showed a degradation of only 4 mV in half-wave potential measurements, whereas the PtNTs and Pt/C showed regressions of 9 and 19 mV, respectively, over the cycling period. In addition, their MA and SA values were measured after the accelerated durability test. The MA and SA of the PABNTs decreased by 9.1%, whereas those values of the Pt/C and PtNTs decreased by 27.2 and 18.8%, respectively (Figure 5C,D). The MA of the PABNTs is 2.18- and 1.36-fold that of the Pt/C and PtNTs, respectively, and the SA of the PABNTs is 6.70- and 1.64-fold that of the Pt/C and PtNTs, respectively. It is obvious that the stability of the PABNTs is much higher than that of the PtNTs and Pt/C. Figure S7 (see the Supporting Information) shows an image of the PABNTs after these cycles. The 1D morphology was maintained, even though a certain ripening had occurred for its high surface energy. The advantages of the 1D nanostructures may contribute to the better performance of the PABNTs. For example, self-supported electrocatalysts avoid the corrosion of the carbon support and the loss of relevant PtNPs,[24,26] and these catalysts could also maintain the improved electron-transport characteristics.[41] Moreover, the alloying of Au with Pt in the nanotubes can change the availability of the active surface sites, thus improving the catalytic activity.[2,9,42,43] In addition, the heterostructures that include a Au component may contribute to a better electrocatalytic performance.[11,22,44]

Conclusion

An intermediate-template-directed method has been developed for the synthesis of novel Pt-based HNCs through the heterogeneous nucleation and growth of Au on Te/Pt core–shell nanostructures in aqueous solution. The synthesized PABNTs consist of porous tubular framework and attached NPs, in which the size of the particles can be adjusted easily by regulating the amount of Au precursor. The PABNTs with an atom ratio of Pt/Au of 7:1 showed an enhanced activity and durability toward the ORR in 0.1 M $HClO_4$ relative to porous PtNTs and commercial Pt/C. The MA of PABNTs was 218% that of commercial Pt/C after an accelerated durability test. This study has demonstrated the potential of PABNTs as highly efficient catalysts as devices for the conversion of chemical→electrical energy, such as PEMFC. More importantly, this study has provided a facile method for the synthesis of other desired HNCs, in which the size and shape is controlled by utilizing intermediate templates.

Experimental Section

Materials and reagents

Tellurium dioxide powder (TeO_2, 99.99%) was purchased from the Aladdin Chemistry Co., Ltd. Hexadecyltrimethylammonium bromide (CTAB, 99%) and sodium dodecyl sulfate (SDS, 99%) were purchased from Sigma–Aldrich. Hydrazine monohydrate (85%, AR), potassium hexachloroplatinate (K_2PtCl_6, AR), tetrachloroauric(III) acid hydrate ($HAuCl_4{\cdot}4H_2O$, AR), methanol (CH_3OH, 99.7%), perchloric acid ($HClO_4$, 70%), and sodium hydrate (NaOH, AR) were supplied by the Sinopharm Chemical Reagent Co., Ltd. Ultrapure water with a conductivity of 18.25 MΩ cm was used throughout the experiments, and all the chemicals were used without further purification.

Synthesis of Te nanowires

TeNWs were prepared according to the method reported by Chang et al.[39] Typically, hydrazine monohydrate (10 mL) was added to a beaker containing tellurium dioxide (0.032 g) at room temperature with constant magnetic stirring. The solution changed from colorless to blue after 50 min, thus indicating the formation of TeNWs. The mixture was diluted tenfold with SDS (10 mM), to terminate the reaction and stabilize the TeNWs, and was then subjected to a centrifugation/wash cycle to remove most of the matrices, including SDS and hydrazine.

Synthesis of porous Au/PtAu bimetallic nanotubes

In a typical synthesis, the thus-obtained TeNWs (ca. 0.04 mmol) were dispersed in an aqueous solution of CTAB (5 mM, 100 mL) with constant magnetic stirring at 30 °C. An aqueous solution of NaOH (0.1 M, 0.4 mL) and K_2PtCl_6 (ca. 0.01 mmol) was added to the solution of CTAB after 30 min. The solution changed from blue to grey–black after 30 min, thus indicating the formation of Te/Pt core–shell nanostructures. $HAuCl_4$ (ca. 2.0 or 0.5 μmol) was added to the solution of CTAB. The solution turned gray–black after 25 min, thus indicating the formation of PABNTs. The mixture was subjected to a centrifugation/wash cycle to remove most of the matrices.

Synthesis of porous Pt nanotubes

Briefly, TeNWs (ca. 0.05 mmol) were dispersed in an aqueous solution of CTAB (5 mM, 100 mL) with constant magnetic stirring. An aqueous solution of NaOH (0.1 M, 0.4 mL) and K_2PtCl_6 (ca. 0.01 mmol) was added to the solution of CTAB after 30 min. The mixture was subjected to a centrifugation/wash cycle after 30 min to remove most of the matrices, redispersed in water, and maintained at room temperature for 3 h. Porous PtNTs were obtained after a centrifugation/wash cycle.

Preparation of the electrodes

All the ORR electrochemical measurements were conducted in a conventional three-electrode cell that consisted of a glassy carbon (GC) rotating-disk working electrode (RDE, diameter = 5 mm; Pine Research Instrumentation) with a rotation control (MSR; Pine Instruments), a platinum wire counterelectrode, and a Ag/AgCl (saturated KCl) reference electrode by using the CHI 660D electrochemical workstation from CH Instuments, Inc. Before the electrochemical test, the GC electrode was carefully and successively polished with alumina powder of 1.0, 0.3, and 0.05 μm; rinsed with deionized water; and sonicated in 8 M HNO_3 and deionized water, respectively. The electrode was allowed to dry under nitrogen. For all the electrochemical tests, the PABNTs (20 μL) and commercial Pt/C catalyst (JM; 20 wt.% Pt, diameter = 3.5 nm) in aqueous solution was dropped on the surface and dried at room temperature. Nafion (3 μL, 0.28%, diluted from 5%; Aldrich) was dropped on each electrode and dried before the electrochemical experiments. The amount of noble-metal loading on each RDE was 14.30, 13.80, and 15.00 μg for the PABNTs, PtNTs, and Pt/C, respectively.

Electrochemical measurements

All of the ORR current densities were normalized to the geometric area of the GC electrode (0.196 cm^2). For the ECSA study, the working electrode was first cycled from −0.2 to 1.0 V versus Ag/AgCl at 100 $mV s^{-1}$ for 50 cycles to clean the surface of the electrode, then the cyclic voltammetry (CV) was measured in an N_2-purged aqueous solution of 0.1 M $HClO_4$ at room temperature versus Ag/AgCl at a scan rate of 50 $mV s^{-1}$.

The ORR tests were conducted in an O_2-saturated aqueous solution of 0.1 M $HClO_4$ at a sweep rate of 10 $mV s^{-1}$ and rotation disk speed of 1600 rpm. The current densities of the prepared catalysts were measured to confirm that they had reached the diffusion limit of about 6 $mA cm^{-2}$ by increasing the mass amount of Pt. In this way, mass-transport was not an issue in these measurements.

The accelerated durability tests were conducted at ambient room temperature by applying potential cycles sweeps between 0.4 and 0.8 V for 10000 cycles at a scan rate of 100 $mV s^{-1}$ in O_2-saturated aqueous solutions of 0.1 M $HClO_4$, while CV curves between −0.2 and 1.0 V and LSV curves from 0.9 to 0 V were recorded to compare the ECSA and ORR activities of different electrocatalysts during the potential cycling.

Characterization

TEM measurements were made on a JEM-2100F high-resolution transmission electron microscope at an accelerating voltage of 200 kV. Scanning transmission electron microscopy (STEM), elemental maps, and cross-sectional line profiles were carried out under the high-angle annular dark-field (HAADF) mode on a FEI TECNAIF-30 microscope operated at 300 kV. Samples for TEM analysis were prepared by depositing a single drop of a dispersion of a nanostructure diluted in water on copper grids. XRD analysis was carried out on a Bruker D8 Advance X-ray diffractometer with $Cu_{K\alpha}$ radiation. Inductively coupled plasma atomic emission spectroscopy (ICP-AES) measurements were performed on IRIS Intrepid II XSP (Thermo Fisher Scientific, USA). UV/Vis absorption spectra were recorded on Nicolet Evolution 300 UV/Vis spectrometer. All the ORR electrochemical measurements were conducted in a conventional three-electrode cell that consisted of a GC RDE (diameter = 5 mm; Pine Research Instrumentation) with a rotation control (MSR; Pine Instruments), a platinum wire counterelectrode, and a Ag/AgCl (saturated KCl) reference electrode by using the CHI 660D electrochemical workstation from CH Instruments, Inc.

Acknowledgements

The authors acknowledge financial support from the National Natural Science Foundation of China (21375043, 21175051) and the Doctor Innovation Project of Huazhong Agricultural University (0900205179).

Keywords: nanotubes · oxygen · platinum · reduction · synthesis design

[1] R. Costi, A. E. Saunders, U. Banin, *Angew. Chem. Int. Ed.* **2010**, *49*, 4878–4897; *Angew. Chem.* **2010**, *122*, 4996–5016.
[2] L. Carbone, P. D. Cozzoli, *Nano Today* **2010**, *5*, 449–493.
[3] X. Feng, G. Hu, J. Hu, *Nanoscale* **2011**, *3*, 2099–2117.
[4] A. Walther, A. H. E. Müller, *Chem. Rev.* **2013**, *113*, 5194–5261.
[5] C. Wang, C. Xu, H. Zeng, S. Sun, *Adv. Mater.* **2009**, *21*, 3045–3052.
[6] J. Wu, Y. Hou, S. Gao, *Nano Res.* **2011**, *4*, 836–848.
[7] B. Lim, Y. Xia, *Angew. Chem. Int. Ed.* **2011**, *50*, 76–85; *Angew. Chem.* **2011**, *123*, 78–87.
[8] S. Zhang, X.-Z. Yuan, J. N. C. Hin, H. Wang, K. A. Friedrich, M. Schulze, *J. Power Sources* **2009**, *194*, 588–600.
[9] S. Guo, E. Wang, *Nano Today* **2011**, *6*, 240–264.
[10] H. Zhang, M. Jin, Y. Xia, *Chem. Soc. Rev.* **2012**, *41*, 8035–8049.
[11] J. Wu, H. Yang, *Acc. Chem. Res.* **2013**, *46*, 1848–1857.

[12] H. Wang, L. Wang, T. Sato, Y. Sakamoto, S. Tominaka, K. Miyasaka, N. Miyamoto, Y. Nemoto, O. Terasaki, Y. Yamauchi, *Chem. Mater.* **2012**, *24*, 1591 – 1598.
[13] H. Ataee-Esfahani, Y. Nemoto, L. Wang, Y. Yamauchi, *Chem. Commun.* **2011**, *47*, 3885 – 3887.
[14] Y. Yamauchi, *J. Ceram. Soc. Jpn.* **2013**, *121*, 831 – 840.
[15] G. Zhang, S. Sun, M. Cai, Y. Zhang, R. Li, X. Sun, *Sci. Rep.* **2013**, *3*, 1526.
[16] Z. Peng, H. Yang, *Nano Today* **2009**, *4*, 143 – 164.
[17] L. Wang, Y. Nemoto, Y. Yamauchi, *J. Am. Chem. Soc.* **2011**, *133*, 9674 – 9677.
[18] Z. Peng, H. Yang, *J. Am. Chem. Soc.* **2009**, *131*, 7542 – 7543.
[19] B. Lim, M. Jiang, P. H. C. Camargo, E. C. Cho, J. Tao, X. Lu, Y. Zhu, Y. Xia, *Science* **2009**, *324*, 1302 – 1305.
[20] Y. Kim, J. W. Hong, Y. W. Lee, M. Kim, D. Kim, W. S. Yun, S. W. Han, *Angew. Chem. Int. Ed.* **2010**, *49*, 10197 – 10201; *Angew. Chem.* **2010**, *122*, 10395 – 10399.
[21] Y. Tan, J. Fan, G. Chen, N. Zheng, Q. Xie, *Chem. Commun.* **2011**, *47*, 11624 – 11626.
[22] J. Zhang, K. Sasaki, E. Sutter, R. R. Adzic, *Science* **2007**, *315*, 220 – 222.
[23] S. Guo, J. Li, S. Dong, E. Wang, *J. Phys. Chem. C* **2010**, *114*, 15337 – 15342.
[24] Z. Chen, M. Waje, W. Li, Y. Yan, *Angew. Chem. Int. Ed.* **2007**, *46*, 4060 – 4063; *Angew. Chem.* **2007**, *119*, 4138 – 4141.
[25] L. Chen, L. Kuai, X. Yu, W. Li, B. Geng, *Chem. Eur. J.* **2013**, *19*, 11753 – 11758.
[26] S. M. Alia, G. Zhang, D. Kisailus, D. Li, S. Gu, K. Jensen, Y. Yan, *Adv. Funct. Mater.* **2010**, *20*, 3742 – 3746.
[27] S. Guo, S. Dong, E. Wang, *Energy Environ. Sci.* **2010**, *3*, 1307 – 1310.
[28] S. Guo, S. Dong, E. Wang, *Chem. Commun.* **2010**, *46*, 1869 – 1871.
[29] J. Mao, X. Cao, J. Zhen, H. Shao, H. Gu, J. Lu, J. Y. Ying, *J. Mater. Chem.* **2011**, *21*, 11478 – 11481.
[30] T. Kijima, T. Yoshimura, M. Uota, T. Ikeda, D. Fujikawa, S. Mouri, S. Uoyama, *Angew. Chem. Int. Ed.* **2004**, *43*, 228 – 232; *Angew. Chem.* **2004**, *116*, 230 – 234.
[31] K. Cai, Z. Lv, K. Chen, L. Huang, J. Wang, F. Shao, Y. Wang, H. Han, *Chem. Commun.* **2013**, *49*, 6024 – 6026.
[32] C. Zhu, S. Guo, S. Dong, *Adv. Mater.* **2012**, *24*, 2326 – 2331.
[33] H.-W. Liang, S. Liu, J.-Y. Gong, S.-B. Wang, L. Wang, S.-H. Yu, *Adv. Mater.* **2009**, *21*, 1850 – 1854.
[34] Z. Huang, H. Zhou, F. Sun, C. Fu, F. Zeng, T. Li, Y. Kuang, *Chem. Eur. J.* **2013**, *19*, 13720 – 13725.
[35] A. K. Samal, T. Pradeep, *Langmuir* **2010**, *26*, 19136 – 19141.
[36] Z.-H. Lin, M.-H. Lin, H.-T. Chang, *Chem. Eur. J.* **2009**, *15*, 4656 – 4662.
[37] Y. Zuo, K. Cai, L. Wu, T. Li, Z. Lv, J. Liu, K. Shao, H. Han, *J. Mater. Chem. A* **2015**, *3*, 1388 – 1391.
[38] C. Zhu, S. Guo, S. Dong, *J. Mater. Chem.* **2012**, *22*, 14851 – 14855.
[39] Z.-H. Lin, Z. Yang, H.-T. Chang, *Cryst. Growth Des.* **2008**, *8*, 351 – 357.
[40] H.-W. Liang, X. Cao, F. Zhou, C.-H. Cui, W.-J. Zhang, S.-H. Yu, *Adv. Mater.* **2011**, *23*, 1467 – 1471.
[41] C. Li, T. Sato, Y. Yamauchi, *Angew. Chem. Int. Ed.* **2013**, *52*, 8050 – 8053; *Angew. Chem.* **2013**, *125*, 8208 – 8211.
[42] C. Wang, N. M. Markovic, V. R. Stamenkovic, *ACS Catal.* **2012**, *2*, 891 – 898.
[43] H.-L. Jiang, Q. Xu, *J. Mater. Chem.* **2011**, *21*, 13705 – 13725.
[44] F. Ye, F. Ye, H. Liu, W. Hu, J. Zhong, Y. Chen, H. Cao, J. Yang, *Dalton Trans.* **2012**, *41*, 2898 – 2903.

Received: December 20, 2014
Published online on April 1, 2015